Korean J. Chem. Eng., 34(11), 2832-2839 (2017)
DOI: 10.1007/s11814-017-0195-x

pISSN: 0256-1115
eISSN: 1975-7220

Particle deposition behaviors of monolithic De-NO_x catalysts for selective catalytic reduction (SCR)

Hongke Feng, Chunhua Wang†, and Ying Huang

College of Energy and Power Engineering, Nanjing University of Aeronautics and Astronautics, Nanjing 210016, China
(*Received 22 March 2017 • accepted 8 July 2017*)

Abstract−A major issue when using selective catalytic reduction (SCR) De-NO_x catalysts is the risk of physical deactivation due to particle deposition and plugging of the monolithic catalysts. In the present study, numerical computations were carried out to investigate the particle deposition behaviors in monolithic SCR catalysts. Based on the calculation results, the effects of particle diameter, particle density, gas velocity, turbulent intensity, chemical reaction and channel size on particle deposition were analyzed in detail. Increasing gas velocity and equivalent diameter of channel can mitigate particle deposition. The increases of turbulent intensity and channel length both lead to the rise of particle deposition ratio. For particles with high Stokes number, particle deposition mainly takes place in the inlet section of catalysts. For particles with low Stokes number, sediment can be observed in the middle and outlet sections of catalysts. De-NO_x chemical reaction can mitigate particle deposition, but the effect of chemical reaction on particle deposition is inactive.

Keywords: SCR De-NO_x Catalyst, Particle, Deposition, Computational Fluid Dynamics

INTRODUCTION

Nitrogen oxides (NO_x) are one of the major air pollutants, which are produced from the reaction of nitrogen and oxygen gases in the air during combustion. Selective catalytic reduction (SCR) of NO_x with ammonia is the most effective and commercially proven technology to remove NO_x [1]. In the SCR De-NO_x process, ammonia or urea is injected in the flue gas, allowing for reactions between NO_x and ammonia into harmless water and nitrogen over a catalyst. The De-NO_x efficiency for commercial SCR catalysts can reach more than 90% [2,3]. In addition to coal-fired power plants, SCR applications also include industrial boilers, marine diesel engines, diesel locomotives, gas turbines and automobiles.

When using selective catalytic reduction (SCR) De-NO_x catalyst, an issue is the risk of physical deactivation due to particle deposition and plugging of the monolithic catalysts. The particulate problem for SCR catalysts is particularly serious in coal-fired power plants. In power plants, the high-dust position of SCR catalysts between the economizer and air preheater is the most commonly used configuration, where the concentration of fly ash can reach more than 20 g/Nm^3 [4]. Even for the low dust application of SCR reactor (the particle concentration is much lower than 20 mg/Nm^3), severe plugging is occasionally observed. The particulate problem is attracting more and more attention from the academic and industrial worlds [4,5].

The different particle transport and deposition mechanisms that are potentially active in a monolithic catalyst are the following: Brownian diffusion, turbulent diffusion, turbophoresis, inertial transport, thermophoresis, shear-induced lift, electrostatic force, drag force and gravity force [6,7]. In these mechanisms, inertial impact plays an important role in the deposition behavior at the inlet region of catalyst; turbulence and Brownian diffusion have a dominant effect in the catalyst channel, and the effects of Brownian diffusion and Saffman lift on deposition are very active at the outlet region [8,9]. Strom et al. [10,11] studied the effects of the turbulent-to-laminar transition at the inlet of a monolithic reactor on the conversion of gaseous species and particle deposition. They identified two main effects of turbulence on gas conversion and particle deposition: slow fluctuations due to turbulent eddy with large scale and rapid fluctuations due to turbulent eddy with small scale. The effects of turbulent-to-laminar transition on gas conversion were also proven by Tanno et al. [12]. The extent of particle deposition depends on particle properties, the shape of catalyst channel, gas velocity, and flow angle, among others. To design efficient De-NO_x systems and mitigate particulate deposition, it is important to know the detailed effects of these parameters on particulate deposition to predict deposition development.

In the present study, the governing equations for gas and solid phase were introduced first, and then the model for particle deposition in SCR monolithic catalyst was established and validated; finally, the effects of particle diameter, particle density, gas velocity, turbulent intensity, chemical reaction and channel size on particle deposition were discussed in detail.

GOVERNING EQUATIONS FOR GAS AND PARTICLE FLOW

1. Gas Phase

The governing equations for mass, momentum, and energy balances for gas phase at steady state are expressed by:

$$\nabla \cdot (\rho_f \mathbf{u}_f) = 0 \tag{1}$$

$$\nabla \cdot (\rho_f \mathbf{u}_f \mathbf{u}_f) = \nabla (\mu_f \nabla \cdot \mathbf{u}_f) - \nabla p \tag{2}$$

†To whom correspondence should be addressed.
E-mail: chunhuawang@nuaa.edu.cn

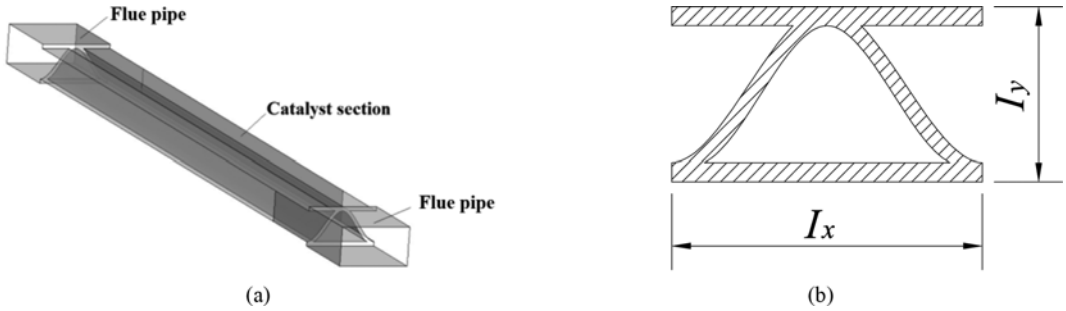

Fig. 1. Geometry of computational domain. (a) 3D view (b) cross-section of catalyst.

$$\nabla\cdot(\rho_f C_{pf} T_f \mathbf{u}_f) = \nabla\cdot(k_f \nabla T_f) - p\nabla\cdot\mathbf{u}_f \tag{3}$$

A species transport equation can be modeled as:

$$\mathbf{u}_f \nabla\cdot y_i = D_{i,N_2}\nabla^2 y_i \tag{4}$$

where, i=NO, NH_3, O_2 and H_2O, and y_i denotes the mass fraction of species i.

For coating catalysts with washcoat thickness less than 0.1 mm, the catalyst layer and inner wall of monolith channels can be taken on as overlapped [13]. Therefore, in the present study, the surface reaction at the boundary condition was specified. The NH_3-SCR $DeNO_x$ reaction catalyzed by V_2O_5-WO_3/TiO_2 follows the Eley-Rideal mechanism. The equation of the overall reaction can be expressed by [14-16]:

$$4NO + 4NH_3 + O_2 \rightarrow 4N_2 + 6H_2O \tag{5}$$

As the O_2 concentration is higher than 2% and NH_3/NO volume ratio is higher than 1, the reaction rate of SCR $DeNO_x$ process can be modeled as:

$$r = kC_{NO} \tag{6}$$

where, C_{NO} is the concentration of NO. k is determined by the empirical correlation [17]:

$$\ln(k) = -6683.6/T_f + 14.626 \tag{7}$$

The binary diffusion coefficients D_{i,N_2} can be modeled by:

$$D_{i,N_2} = \frac{1.43\times10^{-7} T_f^{1.75}(1/M_i + 1/M_{N_2})^{0.5}}{P(V_i^{1/3} + V_{N_2}^{1/3})^2} \tag{8}$$

where, V_i denotes molecular diffusion volume of gas component, and M_i denotes molecular mass.

2. Particle Phase

The governing equation for particle phase can be modeled as:

$$m_p \frac{d\mathbf{u}_p}{dt} = \mathbf{F}_{gp} + \mathbf{G}_p \tag{9}$$

where, $\mathbf{F}_{gp}$ denotes gas-solid interaction force. In the present study, drag force, Buoyance force, Saffman lift force, Brownian force, electrostatic force, and thermophoretic force were taken into account. The mathematical models recommended by Heiredal [18] were used for calculating these forces.

The condition for adhesion of a particle is that the particle-wall contacting velocity is smaller than the critical particle velocity. Heiredal [18] proposed an improved model for calculating the critical velocity based on the research of Heinl and Bohnet [19]:

$$u_{p,crtic} = \sqrt{\left(\frac{h\overline{\omega}}{K_c d_p 4\pi^2 z_0^2}\right)^2 \frac{3}{4H\rho_p} + \frac{3}{2\pi^2 d_p^2 K_c^2}\frac{1}{\varepsilon_0\rho_p}\left(\frac{2q_2^2}{2z_0 + d_p} - \frac{q_1^2}{l}\right)} \tag{10}$$

where, $h\overline{\omega}$ denotes Liffschitz-van der Waals constant, z_0 denotes separation distance, H denotes strength of the wall material, ε_0 is permittivity of free space and K_c is coefficient of restitution.

COMPUTATIONAL MODEL

The commercial DNX x30 monolithic catalysts produced by Haldor Topsoe Inc. are studied. A schematic of the computation domain is shown in Fig. 1. The inlet gas (ideal gas) consists of 0.04%NO, 0.05%NH_3, 5%O_2, 8%H_2O and N_2. Data used for CFD model are listed in Table 1.

Geometry and mesh grid were generated by using Gambit with structured grids, and Ansys Fluent for solving the governing equations for gas and particles. The k-ε model was applied for solving turbulent flow, and enhanced wall treatment was used for near-wall turbulence modeling. The particles were injected from the inlet surface, and particle initial velocity is equal to gas inlet velocity. The parameters for discrete particle model are listed in Table 2. Scaled residuals of all flow parameters below 10^{-4} and energy imbalances in the entire computational domain less than 10^{-7} were the convergence criteria. The solver finished a single simulation in approximately 1500 iterations. The computations were performed by workstation Dell Z620, and 8 compute nodes (Intel Xero CPU E5-2630) were

Table 1. Data used for CFD model

Parameter	Unit	Value
Length of flue inlet pipe, L_i	mm	100
Length of catalyst section, L_c	mm	300-600
Length of flue outlet pipe, L_o	mm	100
Cross-section of catalyst, $I_x \times I_y$	mm	6.2×3.2 8.2×4.6 10.2×5.7
Gas inlet temperature, T_i	K	490-660
Gas inlet turbulent intensity, Tu		0-8%
Gas outlet pressure, P_o	Pa	101325

Table 2. Parameters for DPM

Parameter	Unit	Value
Particle diameter, d_p	μm	0.04-200
Particle density, ρ_p	kg/m^3	500-2000
Separation distance, z_0	m	4×10^{-15}
Strength of the wall material, H	MPa	250×10^6
Liffschitz-van der Waals constant, $h\overline{\omega}$	J	4×10^{-15}
Coefficient of restitution, K_c	[-]	1

used simultaneously. The clock size of every compute node was 2.6 GHz.

Particle deposition model was validated by the experimental data from Ref. [18] and [20] (shown in Fig. 2 and 3). The model over-predicts the particle deposition rate. In the experimental condition, some of particles deposit on the pipe before reaching catalyst in the experimental condition; however, this condition was not considered in the present model. Moreover, particles sticking to surfaces may be detached from the surface under the effect of gas flow, but the present deposition model does not take this process into account.

PARTICLE DEPOSITION IN CATALYSTS

Fig. 4 shows the gas velocity distribution on the cross sections of SCR catalysts, and the background color represents vortices in the main flow direction. In the inlet region (L=3 mm, L: axial distance from end surface of catalyst inlet), the velocity vectors point to the channel center and the vortices are observed. It is because that the sudden decrease of flow area results in turbulent-to-laminar transition [10]. In the central region (L=250 mm), the velocity vectors are parallel to the channel direction and vortices disappear. In the outlet region (L=497 mm), because of the sudden increase of the flow area, laminar flow transits to turbulent flow, the velocity vectors point to the top edge of catalysts, and vortices can be observed again. Fig. 5 shows effects of gas velocity and turbulent intensity on

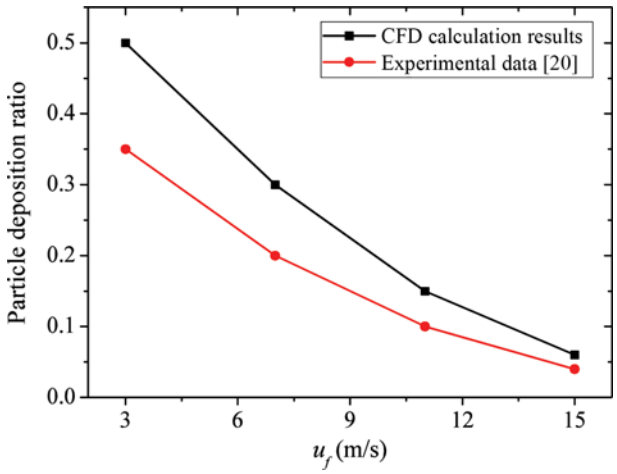

Fig. 3. Validation of particle deposition model by experimental data from Nova [20] (I_x=8.2 mm, I_y=4.6 mm, L_c=600 mm, T_f=293 K, ρ_p=1,500 kg/m^3, d_p=15 μm).

SCR De-NO_x efficiency. As gas velocity increases, the contacting time between catalysts and gas phase decreases, and the De-NO_x efficiency decreases. For turbulent flow, De-NO_x efficiency is higher than that for laminar flow. It is because that turbulent fluctuation promotes the heat transfer and chemical reaction in boundary layers.

Fig. 6 shows the effects of particle diameter and density on particle deposition ratio (the ratio of mass of particle sticking to the surface to the total particle mass flowing). Stokes number of particles, St can be expressed by:

$$St=\frac{\tau U_0}{d_p} \tag{11}$$

$$\tau=\frac{\rho_p d_p^2}{18\mu_f} \tag{12}$$

where, τ is the relaxation time of the particle, and U_0 is the fluid

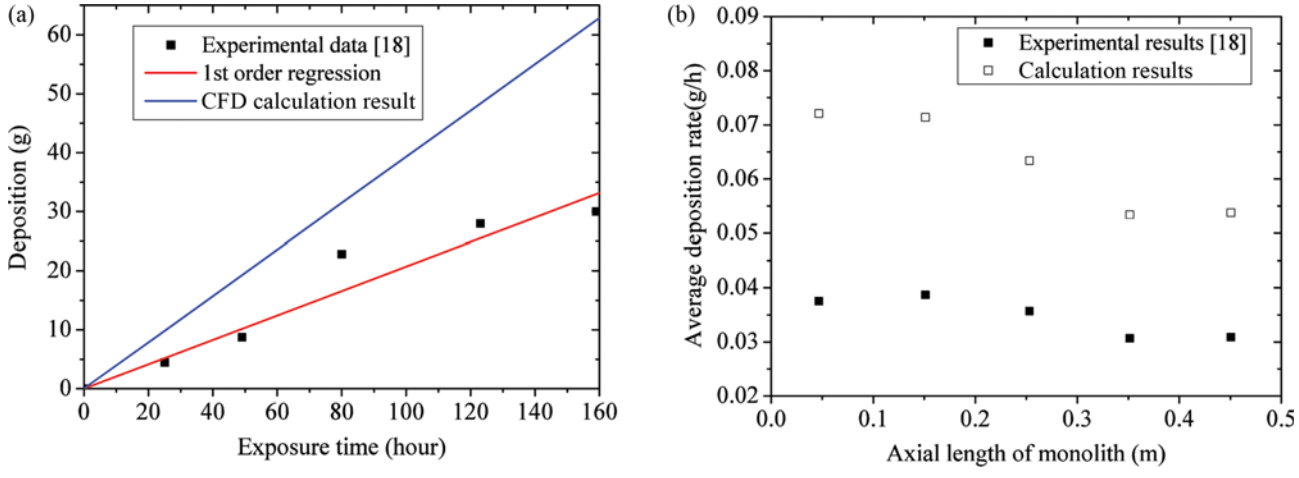

Fig. 2. Validation of particle deposition model by experimental data from Heiredal et al. [18] (I_x=8.2 mm, I_y=4.6 mm, L_c=500 mm, u_f=4.596 m/s, T_f=623 K, ρ_p=1,950 kg/m^3, d_p=0.04-10 μm, $m_{in}=2.1\times10^{-7}$ kg/s). (a) Particle deposition mass (b) distribution of particle deposition rate.

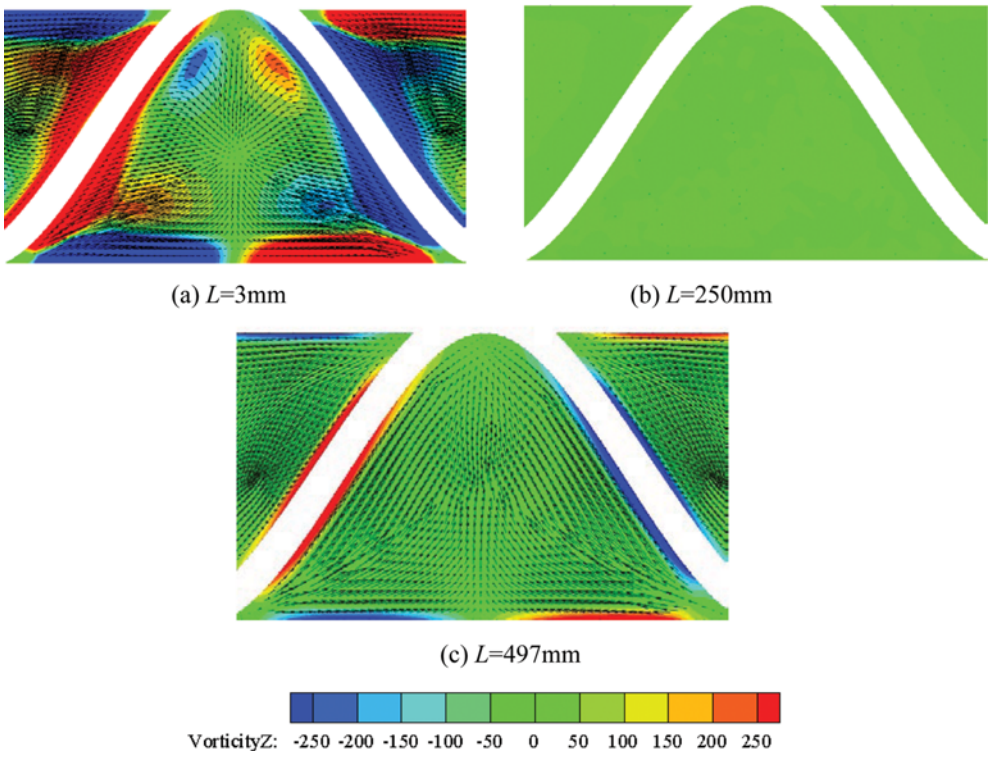

Fig. 4. Velocity distributions on the cross sections of catalyst (I_x=8.2 mm, I_y=4.6 mm, L_c=500 mm, u_f=4.596 m/s, Tu=4%, T_f=623 K).

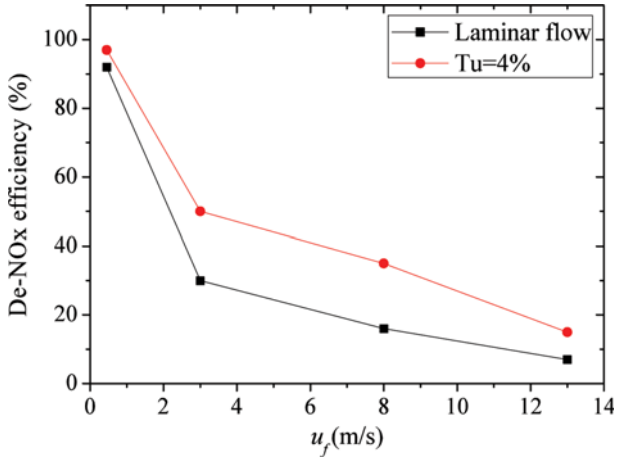

Fig. 5. Effects of gas velocity and turbulent intensity on De-NO_x efficiency (I_x=8.2 mm, I_y=4.6 mm, L_c=500 mm, u_f=4.596 m/s, T_f= 623 K).

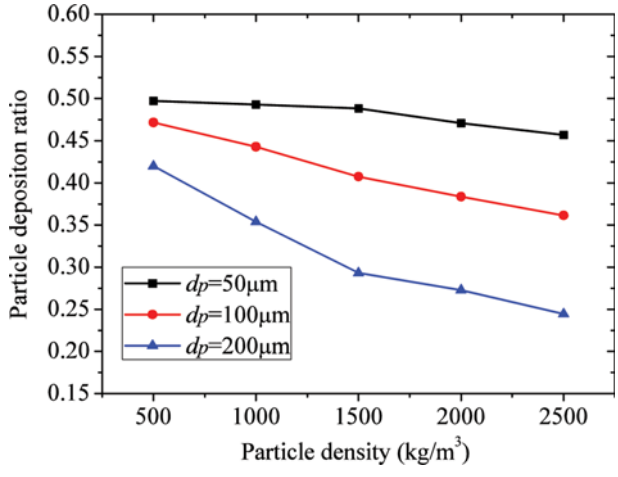

Fig. 6. Effects of particle diameter and density on particle deposition ratio (I_x=8.2 mm, I_y=4.6 mm, L_c=500 mm, u_f=4.596 m/s, Tu=4%, T_f=623 K).

velocity away from the obstacle. As particle density and diameter increase, particle Stokes number increases. For particles with small Stokes number, the particle trajectory is susceptible to fluid stream and particle-wall contacting probability is high. Conversely, for particles with high Stokes number, the particle will continue along its initial trajectory, and particle-wall contacting probability is low [21]. So, particle deposition ratio decreases with the increases of particle density and diameter. Moreover, as particle density or diameter increases, the critical velocity for particle deposition decreases, and reducing the critical velocity mitigates particle deposition.

Fig. 7 shows the distribution of particle concentration in the channel of SCR catalyst. For particles with small Stokes number, particle concentration decreases with the increase of distance from catalyst inlet, which illustrates particle deposition takes place on the inner surface of catalyst. For particles with high Stokes number, particle concentration does not change with distance from catalyst inlet obviously, which illustrates that particles cannot deposit on the inner surface of catalyst. In the channel of monolith catalyst, turbulent and Brownian diffusion are dominant mechanisms for particle deposition [8], but the influence of turbulent diffusion

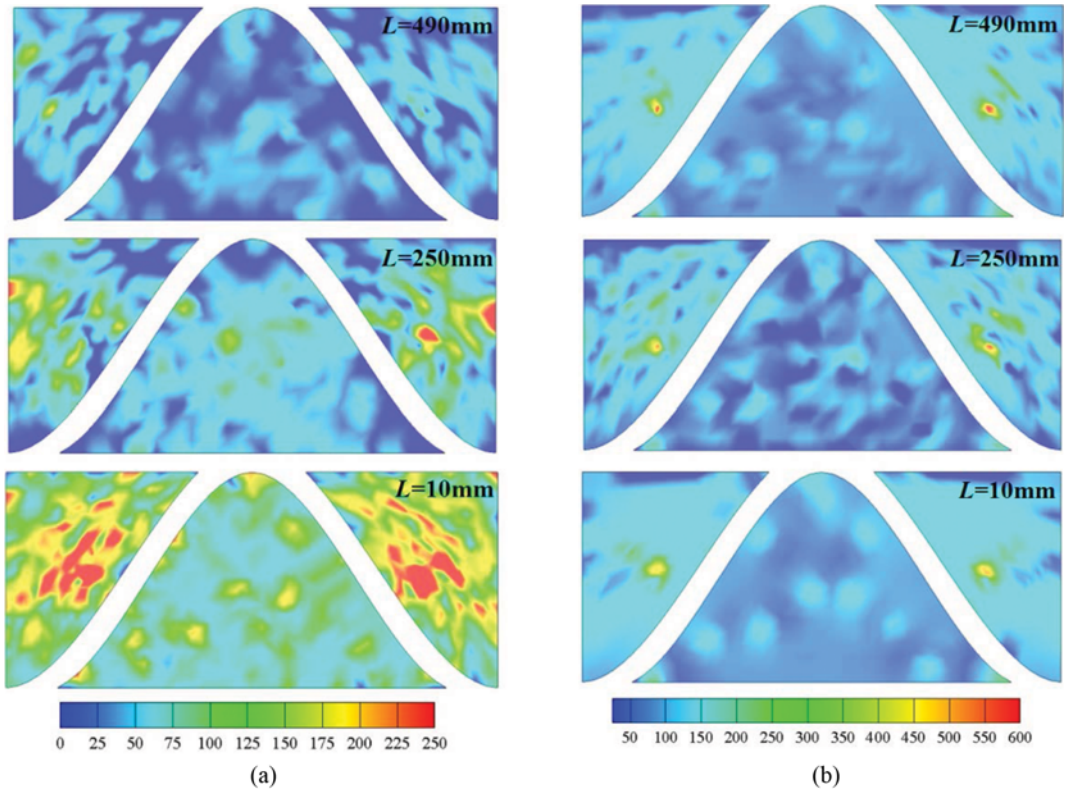

Fig. 7. Distribution of particle concentration inside the channel of catalyst (unit: kg/m^3) (I_x=8.2 mm, I_y=4.6 mm, L_c=500 mm, u_f=4.596 m/s, Tu=4%, T_f=623 K) (a) dp=1 μm, ρ_p=500 kg/m^3, St≈10, (b) dp=200 μm, ρ_p=2,000 kg/m^3, St≈10^4.

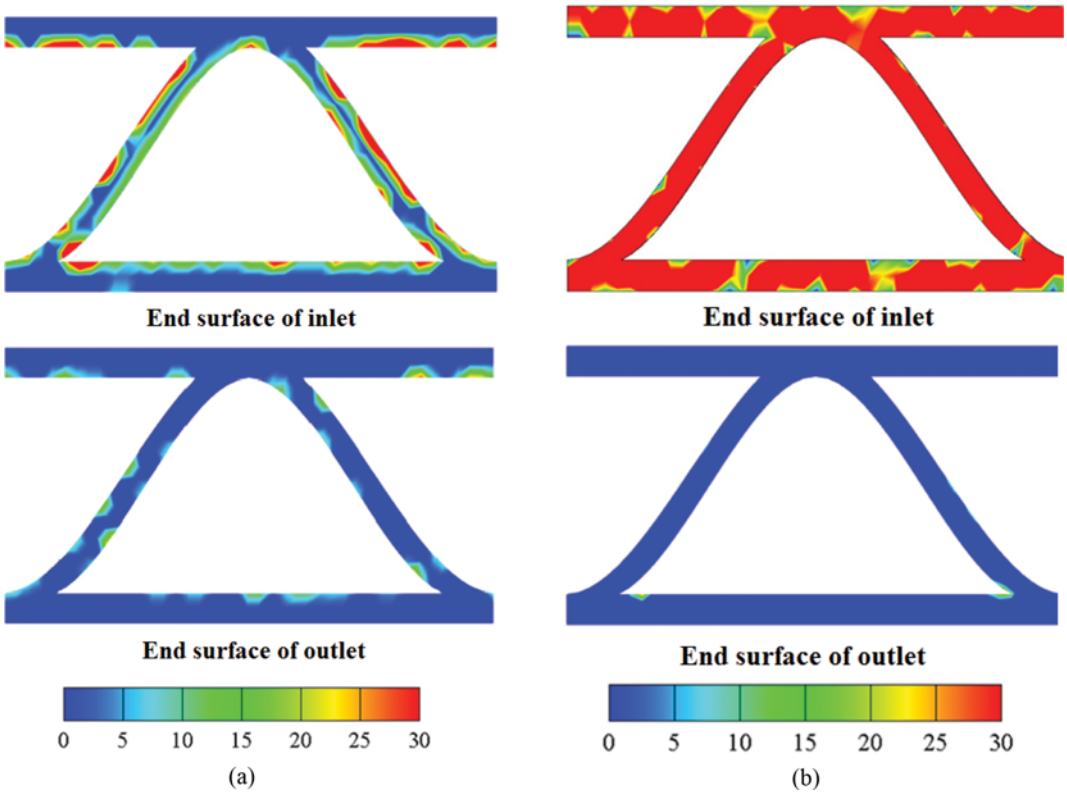

Fig. 8. Distributions of particle concentration on end surfaces of catalyst (unit: kg/m^3) (I_x=8.2 mm, I_y=4.6 mm, L_c=500 mm, u_f=4.596 m/s, Tu=4%, T_f=623 K) (a) dp=1 μm, ρ_p=500 kg/m^3, St≈10, (b) dp=200 μm, ρ_p=2,000 kg/m^3, St≈10^4.

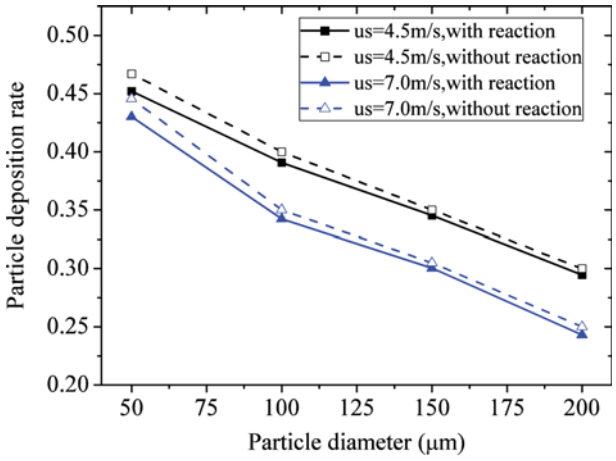

Fig. 9. Effects of gas velocity and SCR-DeNO$_x$ chemical reaction on particle deposition ratio (I_x=8.2 mm, I_y=4.6 mm, L_c=500 mm, Tu=4%, T_f=623 K).

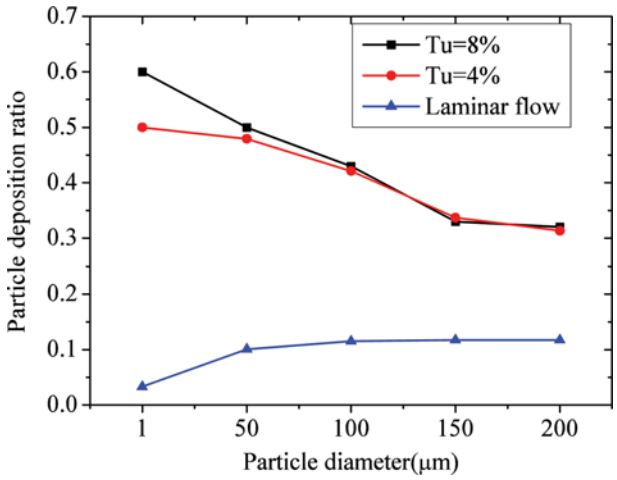

Fig. 11. Effects of turbulent flow on particle deposition ratio (ρ_p= 1,500 kg/m^3, I_x=8.2 mm, I_y=4.6 mm, u_f=4.596 m/s, L_c=500 mm, T_f=623 K).

on the trajectory of particles with high Stokes number is unobvious. Fig. 8 shows the distribution of particle concentration on the end surfaces of SCR catalyst. Particles with high Stokes number mainly deposit on the end surface of catalyst inlet, where inertial impact has a dominant effect. At the end surface of catalyst outlet, sediments of particles with low Stokes number can be observed. It can be attributed to the effects of Brownian diffusion and Saffman lift force.

Fig. 9 shows the effect of gas velocity on particle deposition ratio. Particle deposition ratio decreases by increasing gas velocity. As gas velocity increases, the residual time of gas phase in the channel decreases, which leads to the decrease of particle-wall contacting probability. Moreover, the increase of gas velocity results in the rise of impact velocity of particles on catalysts, which mitigates particle deposition. De-NO$_x$ chemical reaction also has a slight effect on particle deposition. Particle deposition ratio with considering chemical reaction is lower than that without considering chemical reaction. De-NO$_x$ is a typical exothermic reaction, and increasing gas temperature on the boundary region can push particles away from the wall because of the effect of thermophoretic force. However, because that the exothermic effect of De-NO$_x$ chemical reaction is weak, the influence of chemical reaction on particle deposition is not very active.

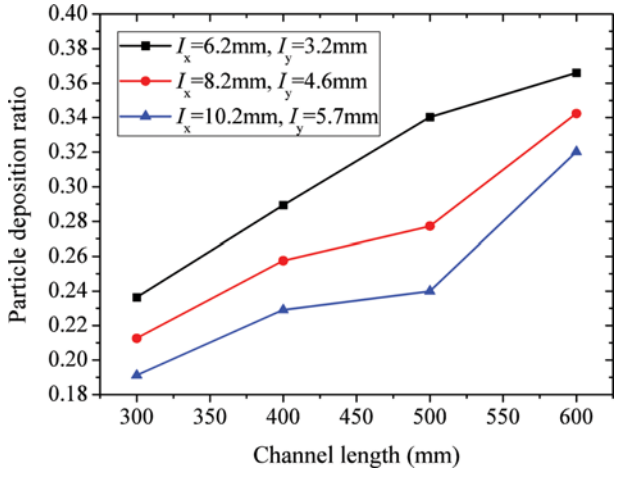

Fig. 10. Effect of cross section size on particle deposition ratio (d_p= 200 μm, ρ_p=1,500 kg/m^3, L_c=500 mm, u_f=4.596 m/s, Tu=4%, T_f=623 K).

Fig. 10 shows the effect of channel size on particle deposition ratio. The rise of channel length results in the increase of the inner area of catalysts, which promotes particle-wall collision. Moreover, as channel length increases, residual time of gas phase in the channel increases, which also promotes particle deposition. The increase of cross-section area results in the decrease of particle-wall collision probability. Therefore, particle deposition ratio decreases with the rise of equivalent diameter of channel.

Fig. 11 shows the effects of turbulence intensity on particle deposition ratio. Without considering turbulent flow, particle deposition ratio increases with the rise of particle diameters. However, as turbulent effect is considered, this changing trend becomes wholly opposite. Moreover, particle deposition ratio with turbulent effect is much higher than that without turbulent effect. However, because particles with high Stokes number are insusceptible to the fluid flow, the effect of turbulent intensity on deposition ratio of particles with high Stokes number becomes inactive as turbulence intensity exceeds 4%. Fig. 12 shows the distribution of particle concentration in the cross sections of catalyst channel. Without turbulent effects, particle concentration does not change with the distance from catalyst inlet, and particle deposition mainly takes place in the inlet section of catalysts. As turbulent effect is considered, particle concentration decreases with the increase of the distance from catalyst inlet, and particles can deposit on the middle section of catalysts. The simulation results support the viewpoint that particle deposition in the catalyst channel is dominated by turbulent spreading of particles.

CONCLUSIONS

CFD was coupled with DPM to investigate the particle deposi-

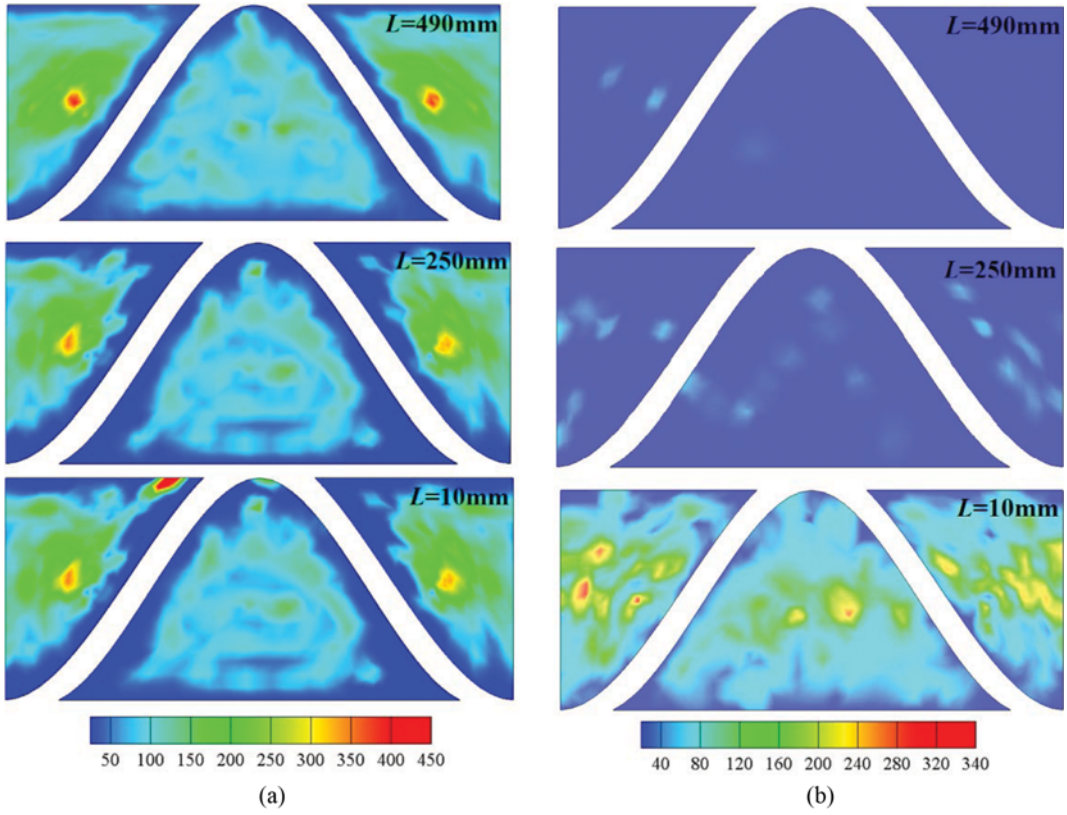

Fig. 12. Distribution of particle concentration inside the channel of catalyst (unit: kg/m^3) (d_p=1 μm, ρ_p=1,500 kg/m^3, u_f=4.596 m/s, I_x=8.2 mm, I_y=4.6 mm, L_c=500 mm, T_f=623 K) (a) Laminar flow, (b) Tu=4%.

tion behavior in monolithic SCR De-NO_x catalysts. The effects of particle diameter, particle density, gas velocity, turbulent intensity, chemical reaction and channel size on particle deposition were investigated. Some useful conclusions were gained as follows:

1) Increasing particle size and density can both mitigate particle deposition. For particles with high Stokes number, particle deposition mainly takes place in the inlet section of SCR catalysts. For particles with low Stokes number, sediments can be observed in the middle and outlet sections of catalysts.

2) Particle deposition ratio decreases with the increase of gas inlet velocity. SCR-DeNO_x chemical reaction is a typical exothermic reaction, and mitigates particle deposition. However, the effect of chemical reaction on particle deposition is not very active.

3) The increase of catalyst length promotes particle deposition. The rise of equivalent diameter of catalyst channel results in decrease of particle deposition ratio.

4) Turbulent flow plays an important role in particle deposition process. Without taking turbulence into account, the particle deposition ratio increases with the rise of particle diameters. However, as turbulence is considered, this changing trend becomes opposite. Particle deposition ratio with considering turbulence is much higher than that without considering turbulent effect.

ACKNOWLEDGEMENTS

The authors thank the Natural Science Fund Program of Jiangsu Province (BK20150749), the Policy-induced Project of Jiangsu Province for the Industry-University-Research Cooperation (BY2015070-21), and Postdoctoral Science Foundation of China (2015M570448) for financial support.

NOMENCLATURE

C_{pf} : specific heat at constant pressure for gas phase [J·kg^{-1}·K^{-1}]
C_{NO} : concentration of NO [mol·m^{-3}]
d_p : particle diameter [m]
D_{i,N_2} : equivalent diffusive coefficient
F_{gp} : gas-particle interaction force [N]
G_p : gravity [N]
$h\overline{\omega}$: Liffschitz-van der Waals constant [J]
H : strength of the wall material [MPa]
k : reaction constant
K_c : coefficient of restitution
k_f : thermal conductivity for gas phase [W m^{-1} K^{-1}]
l : distance from particle to wall [m]
L : distance to catalyst inlet [m]
L_i : length of inlet section of catalyst [m]
L_c : length of catalyst section [m]
L_o : length of outlet section of catalyst [m]
M_i : molecular mass of species i [kg]
m_{in} : particle mass flow rate [kg s^{-1}]
m_p : particle mass [kg]
p : pressure [Pa]
q_1 : charge on particle before wall collision [C]

q_2 : charge on particle after wall collision [C]
r : reaction rate
St : particle stokes number
t : reaction time [s]
T_f : gas temperature [K]
Tu : turbulence intensity
u_f : gas velocity [m s^{-1}]
u_p : particle velocity [m s^{-1}]
$u_{p,critic}$: critical velocity for particle deposition [m s^{-1}]
V_i : molecular diffusion volume of species i [m^3]
y_i : mass fraction of species i
z_0 : separation distance [m]
ρ_f : gas density [kg m^{-3}]
ρ_p : particle density [kg m^{-3}]
ε_0 : permittivity of free space
μ_f : dynamic viscosity for gas phase [Pa·s]

REFERENCES

1. S. A. Benson, J. D. Laumb, C. R. Crocker and J. H. Pavlish, *Fuel Process. Technol.*, **86**, 577 (2005).
2. Z. G. Lei, X. Y. Liu and M. R. Jia, *Energy Fuels*, **23**, 6146 (2009).
3. Z. G. Lei, C. P. Wen, J. Zhang and B. H. Chen, *Ind. Eng. Chem. Res.*, **50**, 5942 (2011).
4. L. Czarnecki and P. Oliveira, *Emerging challenges and design strategies for SCR systems*, Proc. of ASME Power Conference, Maryland, U.S.A. (2014).
5. Y. Y. Xu, Y. Zhang, F. N. Liu, W. F. Shi and J. Q. Yuan, *Comput. Chem. Eng.*, **69**, 19 (2014).
6. A. Guha, *J. Aerosol Sci.*, **28**, 1517 (1997).
7. A. Guha, *Annual Review Fluid Mechanics*, **40**, 311(2008).
8. J. Q. E, M. Liu, Y. W. Deng, H. Zhu and J. K. Gong, *Canadian J. Chem. Eng.*, **94**, 168 (2016).
9. J. Q. E, L. F. Xie, Q. S. Zuo and G. J. Zhang, *Atmospheric Pollution Research*, **7**, 9 (2016).
10. H. Strom, S. Sasic and B. Andersson, *Ind. Eng. Chem. Res.*, **50**, 3194 (2011).
11. H. Strom, S. Sasic and B. Andersson, *Chem. Eng. Sci.*, **69**, 231 (2012).
12. K. Tanno, R. Kurose, T. Michioka, H. Makino and S. Komori, *Adv. Powder Technol.*, **23**, 879 (2013).
13. J. Yao, Z. P. Zhong and L. Zhu, *Chem. Eng. Technol.*, **38**, 283 (2015).
14. J. W. Chen, H. Yang, N. Wang, Z. Ring and T. Dabros, *Appl. Catal. A: Gen.*, **345**, 1 (2008).
15. B. Roduit, A. Baiker, F. Bettoni, J. Baldyga and A. Wokaun, *AIChE J.*, **44**, 2731 (1998).
16. R. Khodayari and C. U. I. Odenbrand, *Chem. Eng. Sci.*, **54**, 1775 (1999).
17. J. Yao, Z. P. Zhong and X. Y. Zhang, *Canadian J. Chem. Eng.*, **92**, 803 (2014).
18. M. L. Heiredal, A. D. Jensen, J. R. Thoger, F. J. Frandsen and J. U. Friemann, *AIChE J.*, **59**, 1919 (2013).
19. E. Heinl and M. Bohnet, *Powder Technol.*, **159**, 95 (2005).
20. E. Nova, *Study on particulate problems in SCR honeycomb catalysts*, Master Thesis, University of Colorado, U.S.A. (2007).
21. C. H. Wang, J. Z. Zhou and J. H. Zhou, *Flow Turbulence and Combustion*, **97**, 591 (2016).